DRAFT VERSION JANUARY 24, 2011
Preprint typeset using LaTeX style emulateapj v. 11/10/09

PTF 10BZF (SN 2010AH): A BROAD-LINE IC SUPERNOVA DISCOVERED BY THE PALOMAR TRANSIENT FACTORY

A. CORSI[1], E. O. OFEK[2,3], D. A. FRAIL[4], D. POZNANSKI[3,5,6], I. ARCAVI[7] , A. GAL-YAM[7], S. R. KULKARNI[2], K. HURLEY[8], P. A. MAZZALI[9,10], D. A. HOWELL[11,12], M. M. KASLIWAL[2], Y. GREEN[7], D. MURRAY[11,12], D. XU[7], S. BEN-AMI[7], J. S. BLOOM[6], B. CENKO[6], N. M. LAW[13], P. NUGENT[5,6], R. M. QUIMBY[2], V. PAL'SHIN[14], J. CUMMINGS[15], V. CONNAUGHTON[16], K. YAMAOKA[17], A. RAU[18], W. BOYNTON[19], I. MITROFANOV[20], J. GOLDSTEN[21]

Draft version January 24, 2011

ABSTRACT

We present the discovery and follow-up observations of a broad-line type-Ic supernova (SN), PTF 10bzf (SN 2010ah), detected by the Palomar Transient Factory (PTF) on 2010 February 23. The SN distance is $\cong$ 218 Mpc, greater than GRB 980425 / SN 1998bw and GRB 060218 / SN 2006aj, but smaller than the other SNe firmly associated with gamma-ray bursts (GRBs). We conducted a multi-wavelength follow-up campaign with Palomar-48 inch, Gemini-N, Keck, Wise, *Swift*, the Allen Telescope Array, CARMA, WSRT, and EVLA. Here we compare the properties of PTF 10bzf with those of SN 1998bw and other broad-line SNe. The optical luminosity and spectral properties of PTF 10bzf suggest that this SN is intermediate, in kinetic energy and amount of ^{56}Ni, between non GRB-associated SNe like 2002ap or 1997ef, and GRB-associated SNe like 1998bw. No X-ray or radio counterpart to PTF 10bzf was detected. X-ray upper-limits allow us to exclude the presence of an underlying X-ray afterglow as luminous as that of GRB 980425. Early-time radio upper-limits do not show evidence for mildly-relativistic ejecta. Late-time radio upper-limits rule out the presence of an underlying off-axis GRB, with energy and wind density similar to the SN-associated GRB 030329 and GRB 031203. Finally, by performing a search for a GRB in the time window and at the position of PTF 10bzf, we find that no GRB in the IPN catalog could be associated with this SN.

Subject headings: supernovae: general — supernovae: individual (PTF 10bzf) — Gamma rays: bursts — radiation mechanisms: non-thermal

1. INTRODUCTION

The Palomar Transient Factory[22] (PTF; Law et al. 2009; Rau et al. 2009) is an on-going project optimized for detecting optical transients in the local Universe. One of its main objectives is the collection of a large sample of core-collapse supernovae (SNe; e.g. Arcavi et al. 2010), for which multi-color optical light-curves and spectra can be obtained through dedicated follow-up resources.

The explosive death of a SN massive progenitor occurs when its iron core collapses to a neutron star or a black hole. Core-collapse SNe are either of type Ib/Ic if the Hydrogen envelope of the progenitor is lost, or else of Type II (Filippenko 1997). While the total kinetic energy released in the explosion is of the order of 10^{51} erg, roughly the same as the energy of the jet that makes a gamma-ray burst (GRB), core-collapse SNe are in general not accompanied by highly relativistic mass ejection, and are visible from all angles.

The discovery of an association between a Ic SN and a long duration GRB in 1998 (Galama et al. 1998; Kulkarni et al. 1998), strongly supported the collapsar scenario (e.g. MacFadyen & Woosley 1999; Mészáros 2006; Woosley & Bloom 2006, and references therein). About two and a half days after the detection of GRB 980425 by BeppoSax and BATSE, the bright and spectroscopically peculiar SN 1998bw was discovered in the BeppoSax error box (Galama et al. 1998). This was one of the most unusual Type Ic SNe seen up to that time: the SN bolometric luminosity at peak was of $\approx 1.6\times10^{43}$ erg s^{-1}, much brighter than typical Ic SNe, with broad lines and strong radio emission indicating a relativistic expansion speed ($\sim 0.3c$; Kulkarni et al. 1998). GRB 980425 showed peculiar properties as well, when compared to cosmological long-duration GRBs: at a redshift of $z = 0.0085$, it was the nearest GRB discovered for which the redshift was known; with an isotropic energy release of

[1] LIGO laboratory, California Institute of Technology, MS 100-36, Pasadena, CA 91125, USA; corsi@caltech.edu
[2] Cahill Center for Astrophysics, California Institute of Technology, Pasadena, CA, 91125, USA
[3] Einstein Fellow
[4] National Radio Astronomy Observatory, P.O. Box 0, Socorro, NM 87801, USA
[5] Computational Cosmology Center, Lawrence Berkeley National Laboratory, 1 Cyclotron Road, Berkeley, CA 94720, USA
[6] Department of Astronomy, 601 Campbell Hall, University of California, Berkeley, CA 94720-3411, USA
[7] Department of Particle Physics and Astrophysics, The Weizmann Institute of Science, Rehovot 76100, Israel
[8] Space Sciences Laboratory, University of California Berkeley, 7 Gauss Way, Berkeley, CA 94720, USA
[9] INAF - Osservatorio Astronomico, vicolo dell'Osservatorio, 5, I-35122 Padova, Italy
[10] Max-Planck Institut für Astrophysik, Karl-Schwarzschildstr. 1, D-85748 Garching, Germany
[11] Las Cumbres Observatory Global Telescope Network, Inc, Santa Barbara, CA, 93117, USA
[12] Department of Physics, University of California Santa Barbara, Santa Barbara, CA 93106, USA
[13] Dunlap Institute for Astronomy and Astrophysics, University of Toronto, 50 St. George Street, Toronto M5S 3H4, Ontario, Canada
[14] Ioffe Physico-Technical Institute of the Russian Academy of Sciences, St. Petersburg, Russian Federation
[15] NASA Goddard Space Flight Center, Greenbelt, MD
[16] University of Alabama in Huntsville CSPAR, Huntsville AL
[17] Department of Physics and Mathematics, Aoyama Gakuin University, Kanagawa, Japan
[18] Max-Planck-Institut für extraterrestrische Physik, Garching, Germany
[19] University of Arizona, Department of Planetary Sciences, Tucson, AZ
[20] Space Research Institute, Moscow, Russian Federation
[21] Applied Physics Laboratory, Johns Hopkins University, Laurel, MD

[22] http://www.astro.caltech.edu/ptf/

$\approx 6 \times 10^{47}$ ergs, it was $\sim 10^4$ times less energetic than typical cosmological events.

Since 1998, a total of five reliable associations between GRBs and SNe have been identified (Table 1). However, the GRB-SN connection is not well understood yet, and some long GRBs are clearly not associated with a SN, e.g. GRB 060505 (Ofek et al. 2007) and GRB 060614 (Della Valle et al. 2006; Fynbo et al. 2006; Gal-Yam et al. 2006a). All the SNe which are known to be associated with GRBs belong to a single rare class of events: broad-line Ic SN, characterized by a very large explosion energy. Sometimes they are referred to as "hypernovae". We note, however, that after the discovery of 1998bw, the peculiar Ic SN 1997ef was re-analyzed and recognized to be an hypernovae (e.g. Mazzali et al. 2000): SN 1997ef remains so far the most energetic peculiar Ic SN without a clear GRB association. In addition, SN 2009bb (Soderberg et al. 2010) showed clear evidence of very high expansion velocity (as normally seen in hypernovae), but no clear GRB association.

Because of their low (electromagnetic) luminosity compared to GRBs, usually SNe are observed at non-cosmological distances ($z \lesssim 1$). Thus, broad-line Ib/c represent a tool to search for nearby, off-axis, GRBs and understand their relation with cosmological bursts (e.g. Norris 2002; Podsiadlowski et al. 2004; Guetta & Della Valle 2007; Liang et al. 2007; Virgili et al. 2009). The connection between broad-line Ic SNe and GRBs was investigated by many studies. For example, by using early- and late-time radio observations of Ic SNe (e.g. Berger et al. 2003; Soderberg et al. 2006b; Guetta & Della Valle 2007), and searching for the radio signal from orphan GRBs (e.g. Gal-Yam et al. 2006b; Soderberg et al. 2006b). Based on these studies, we now know that SNe Ic connected to GRB explosions are very rare, less than few percent of the Ic population. However, what makes some broad-line Ic SNe have an accompanying GRB is still a mystery. Therefore, we are monitoring all the broad-line Ic SNe we discover with PTF.

Here, we present the discovery of a broad-line Ic SN, PTF 10bzf (SN 2010ah), detected by PTF. This event is interesting because of two reasons. First, as a broad-line SN located at a distance smaller than most GRB-associated events (except for GRB 980425 / SN 1998bw and GRB 060218 / SN 2006aj, see Table 1). Next, this event enjoyed a rich radio-to-X-ray follow-up campaign. In what follows, we first describe the observations that led to the discovery of PTF 10bzf (§2), and its multi-wavelength follow-up campaign (§3). Then, we compare PTF 10bzf with SN 1998bw and describe the results of an associated GRB search (§4). Finally, we conclude in §5.

2. OBSERVATIONS AND DATA REDUCTION

On 2010 February 23.5038 (hereafter all times are given in UTC), we discovered a broad-line type-Ic SN, PTF 10bzf, visible at a magnitude of $R \simeq 19$ (see Table 2 and Figure 1), in a 60 s exposure image taken with the Palomar 48-inch telescope (P48). The SN was not seen in previous images of the same field taken on 2010 February 19.4392, down to a limiting magnitude of $R > 21.4$. The SN J2000 position is RA=11:44:02.99, Dec=+55:41:27.6 (Ofek et al. 2010), $\cong 5.2''$ offset and at a position angle of $\cong 5$ deg (North through East) about the position of the galaxy SDSS[23] J114402.98+554122.5.

[23] Sloan Digital Sky Survey (York et al. 2000).

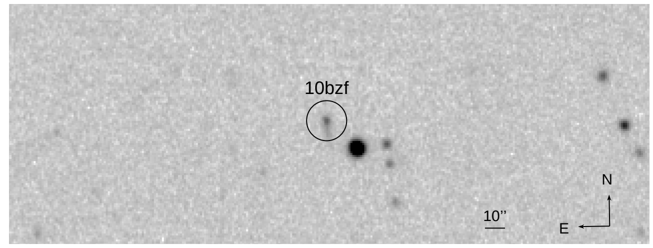

FIG. 1.— Discovery image of PTF 10bzf in the R-band. For clarity purposes, a circle of $10''$ radius marks the position of PTF 10 bzf. The SN is located at RA=11:44:02.99 and Dec=+55:41:27.6 (J2000), and its host galaxy is also visible.

2.1. *Optical photometry*

P48 observations of the PTF 10bzf field were performed with the Mould-R filter. A high-quality image produced by stacking several images of the same field (obtained between May 2009 and June 2009), was used as a reference and subtracted from the individual images. Photometry was performed relative to the r-band magnitude of ten SDSS reference stars in the field, neglecting the color term. All the P48 photometry is listed in Table 2. The P48 calibrated light-curve of PTF 10bzf is plotted in Figure 2.

We also observed the PTF 10bzf field with the 1 m telescope at the Wise observatory[24] using *BVRI* filters (see Table 2). Image subtraction was performed using the common point spread function method via the "mkdifflc" routine (Gal-Yam et al. 2004, 2008). Errors on the Wise data are estimated by using "artificial" sources at a brightness similar to that of the real SN, with the scatter in their magnitudes providing an estimate of the error due to subtraction residuals. The measured magnitude was calibrated against the magnitudes of SDSS stars in the same field (see Figure 7 in the Appendix) using the procedure described in Jordi et al. (2006). Calibration errors were summed in quadrature with the subtraction errors.

2.2. *Spectroscopy*

Gemini North GMOS (Hook et al. 2004) spectra were taken on 2010 March 2, using a $1''$ slit, with the B600 and R400 gratings. Standard data reduction was performed with IRAF V2.14, using the Gemini 1.10 reduction packages. The Gemini spectrum of PTF 10bzf is shown in Figure 3. A redshift of $z = 0.0498$ was derived from the host galaxy emission lines of O III, Hα, Hβ, N II, and S II. The spectrum (black line in Figure 3), resembles that of SN 1998bw at a similar epoch (red line in Figure 3 and Galama et al. 1998), and shows very broad lines, leading us to classify this SN as a broad-line Ic.

Keck data taken on 2010 March 7 (Figure 4), were reduced using the standard longslit reduction packages developed in the IRAF environment.

Both Gemini and Keck spectra were used to derive synthetic photometry in SDSS r-, g-, and i-bands (Table 2).

2.3. *Swift follow-up observations*

A two-epoch observation of PTF 10bzf was performed as part of a *Swift* Target of Opportunity program[25]. *Swift*/XRT did not detect any X-ray counterpart to PTF 10bzf (Kasliwal & Cenko 2010). The corresponding upper limits

[24] http://wise–obs.tau.ac.il/

[25] "Unveiling New Classes of Transients with Palomar Transient Factory", PI S. R. Kulkarni

TABLE 1
SUMMARY OF LIGHT-CURVE PROPERTIES

SN	type	Associated GRB	d_L Mpc	M_R (mag)	$M_{Ni}/M_\odot$
SN 1998bw[a]	engine-driven BL-Ic	GRB 980425	37	-19.36 ± 0.05	$0.4 - 0.5$
SN 2003dh[b]	engine-driven BL-Ic	GRB 030329	810	≈ -19	$0.25 - 0.45$
SN 2003lw[c]	engine-driven BL-Ic	GRB 031203	477	-19.90 ± 0.08	$0.45 - 0.65$
SN 2006aj[d]	engine-driven BL-Ic	GRB 060218	140	-18.81 ± 0.06	0.21
SN 2010dh[e]	engine-driven BL-Ic	GRB 100316D	261	-	-
SN 2009bb[f]	engine-driven BL-Ic	none	40	-18.56 ± 0.28	0.16-0.28
SN 2003jd[g]	BL-Ic	none	78	-18.94 ± 0.30	0.26-0.45
SN 2002ap[h]	BL-Ic	none	7.8	-17.50 ± 0.32	0.06-0.12

NOTE. — See also Woosley & Bloom (2006), and references therein, for a recent review.
[a] Galama et al. (1998); Iwamoto et al. (1998); Nakamura et al. (2001)
[b] Hjorth et al. (2003); Matheson et al. (2003); Deng et al. (2005)
[c] Malesani et al. (2004); Mazzali et al. (2006b)
[d] Mazzali et al. (2006a); Pian et al. (2006); Soderberg et al. (2006a); Valenti et al. (2008)
[e] Starling et al. (2010)
[f] Pignata et al. (2011)
[g] Mazzali et al. (2005); Valenti et al. (2008); Drout et al. (2010)
[h] Gal-Yam et al. (2002); Mazzali et al. (2002); Foley et al. (2003); Drout et al. (2010)

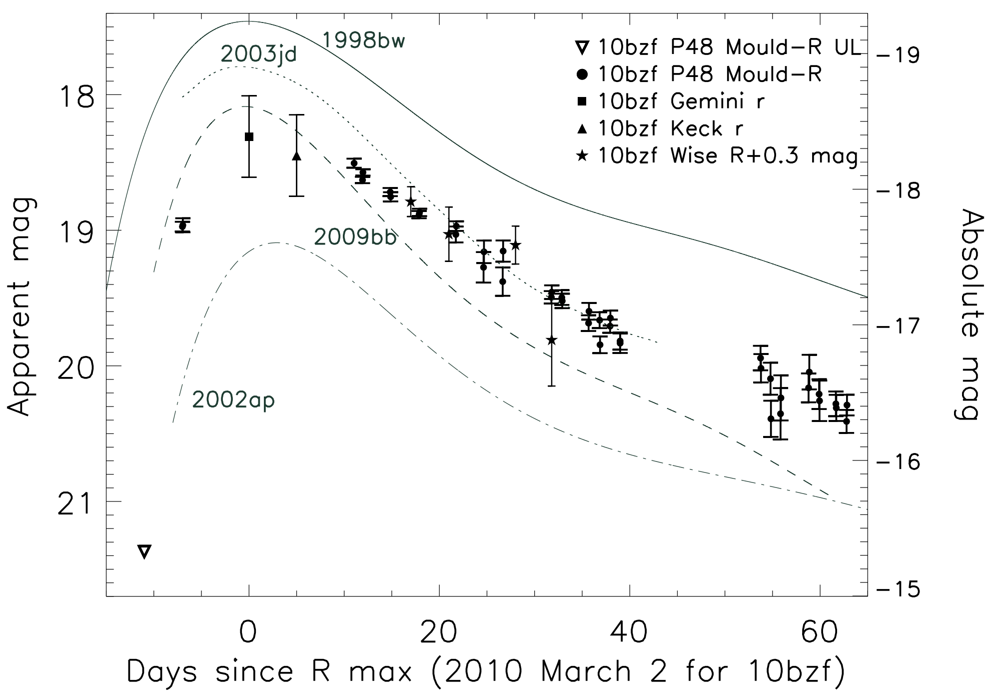

FIG. 2.— Light-curve of PTF 10bzf corrected for Galactic extinction. Absolute magnitudes are plotted on the right axis. P48 data in Mould-R filter and AB system (dots) are calibrated using r-band magnitudes of ten SDSS stars. Synthetic photometry obtained from Gemini (filled square) and Keck (filled triangle) spectra is referred to SDSS r-band and expressed in AB system. From the Gemini spectrum, we estimate $R - r \approx -0.1$ mag for the conversion from SDSS r-band magnitudes in AB system, to R-band magnitudes in Vega system. Wise data in the R filter and Vega system (stars), are calibrated to SDSS as described in Jordi et al. (2006). For comparison with P48 photometry, Wise data are shifted to account for $r - R \approx 0.3$ mag for the conversion from SDSS r-band magnitudes in AB system, to Wise R-band magnitudes in Vega system (Jordi et al. 2006). We also plot the R-band light-curve template of SN 1998bw (solid line), SN 2003jd (dotted line), SN 2009bb (dashed line), and SN 2002ap (dash-dotted line), rescaled to the redshift of PTF 10bzf. These templates are obtained interpolating data retrieved from: Galama et al. (1998) for SN 1998bw; Gal-Yam et al. (2002); Foley et al. (2003) for SN 2002ap; Valenti et al. (2008) for SN 2003jd; Pignata et al. (2011) for SN 2009bb.

TABLE 2
PTF 10BZF FOLLOW-UP CAMPAIGN.

JD-2455251.004 (days since 2010 Feb 23.504)	Telescope	Δt (s)	Band	Mag or Flux	Reference
-4.061 [a]	P48	60	Mould-*R*	> 21.4	ATEL 2470
0.004	P48	60	Mould-*R*	19.00 ± 0.03	ATEL 2470
0.049	P48	60	Mould-*R*	18.99 ± 0.05	This paper
18.042	P48	60	Mould-*R*	18.54 ± 0.03	This paper
18.925	P48	60	Mould-*R*	18.66 ± 0.02	This paper
18.969	P48	60	Mould-*R*	18.60 ± 0.02	This paper
21.836	P48	60	Mould-*R*	18.75 ± 0.03	This paper
21.879	P48	60	Mould-*R*	18.78 ± 0.03	This paper
24.870	P48	60	Mould-*R*	18.91 ± 0.03	This paper
24.914	P48	60	Mould-*R*	18.90 ± 0.03	This paper
28.731	P48	60	Mould-*R*	19.06 ± 0.06	This paper
28.775	P48	60	Mould-*R*	19.00 ± 0.03	This paper
31.640	P48	60	Mould-*R*	19.3 ± 0.1	This paper
31.683	P48	60	Mould-*R*	19.19 ± 0.08	This paper
33.654	P48	60	Mould-*R*	19.4 ± 0.1	This paper
33.699	P48	60	Mould-*R*	19.18 ± 0.08	This paper
38.762	P48	60	Mould-*R*	19.52 ± 0.04	This paper
38.806	P48	60	Mould-*R*	19.49 ± 0.05	This paper
39.861	P48	60	Mould-*R*	19.53 ± 0.05	This paper
39.905	P48	60	Mould-*R*	19.55 ± 0.05	This paper
42.673	P48	60	Mould-*R*	19.72 ± 0.06	This paper
42.717	P48	60	Mould-*R*	19.63 ± 0.06	This paper
43.833	P48	60	Mould-*R*	19.69 ± 0.06	This paper
43.877	P48	60	Mould-*R*	19.87 ± 0.06	This paper
44.930	P48	60	Mould-*R*	19.74 ± 0.05	This paper
44.966	P48	60	Mould-*R*	19.68 ± 0.05	This paper
45.987	P48	60	Mould-*R*	19.85 ± 0.06	This paper
45.988	P48	60	Mould-*R*	19.86 ± 0.07	This paper
60.741	P48	60	Mould-*R*	19.97 ± 0.09	This paper
60.785	P48	60	Mould-*R*	20.0 ± 0.1	This paper
61.786	P48	60	Mould-*R*	20.1 ± 0.1	This paper
61.830	P48	60	Mould-*R*	20.4 ± 0.1	This paper
62.839	P48	60	Mould-*R*	20.4 ± 0.2	This paper
62.882	P48	60	Mould-*R*	20.3 ± 0.2	This paper
65.786	P48	60	Mould-*R*	20.2 ± 0.1	This paper
65.860	P48	60	Mould-*R*	20.1 ± 0.1	This paper
66.892	P48	60	Mould-*R*	20.2 ± 0.1	This paper
66.936	P48	60	Mould-*R*	20.3 ± 0.1	This paper
68.653	P48	60	Mould-*R*	20.31 ± 0.09	This paper
68.696	P48	60	Mould-*R*	20.3 ± 0.1	This paper
69.775	P48	60	Mould-*R*	20.44 ± 0.08	This paper
69.819	P48	60	Mould-*R*	20.32 ± 0.08	This paper
24	Wise (PI)	600	*B*	20.34 ± 0.57[a]	This paper
24	Wise (PI)	600	*V*	19.08 ± 0.18[a]	This paper
24	Wise (PI)	600	*R*	18.55 ± 0.11[a]	This paper
28	Wise (PI)	600	*I*	18.42 ± 0.20[a]	This paper
28	Wise (PI)	600	*B*	20.60 ± 0.64[a]	This paper
28	Wise (PI)	600	*V*	19.36 ± 0.27[a]	This paper
28	Wise (PI)	600	*R*	18.79 ± 0.20[a]	This paper
28	Wise (PI)	600	*I*	18.60 ± 0.13[a]	This paper
35	Wise (LAIWO)	720	*V*	20.27 ± 0.42[a]	This paper
35	Wise (LAIWO)	720	*R*	18.87 ± 0.14[a]	This paper
35	Wise (LAIWO)	720	*I*	19.00 ± 0.61[a]	This paper
38	Wise (LAIWO)	720	*V*	19.87 ± 0.69[a]	This paper
38	Wise (LAIWO)	720	*R*	19.57 ± 0.34[a]	This paper
7	Gemini	450	*g*[b]	18.60 ± 0.3	ATEL 2470
7	Gemini	450	*r*[b]	18.34 ± 0.3	ATEL 2470
7	Gemini	450	*i*[b]	18.66 ± 0.3	ATEL 2470
12	Keck	240	*g*[b]	18.91 ± 0.3	This paper
12	Keck	2×80	*r*[b]	18.48 ± 0.3	This paper
12	Keck	2×80	*i*[b]	18.70 ± 0.3	This paper
8.52	UVOT	5×10^3	*B*	18.73 ± 0.10	ATEL 2471
8.52	UVOT	5×10^3	*U*	18.88 ± 0.12	ATEL 2471
8.52	UVOT	5×10^3	*UVW*1	20.07 ± 0.18	ATEL 2471
8.52	UVOT	5×10^3	*UVW*2	20.18 ± 0.26	ATEL 2471
12.80	UVOT	2.5×10^3	*U*	19.68 ± 0.14	ATEL 2471
12.80	UVOT	2.5×10^3	*UVW*1	20.12 ± 0.24	ATEL 2471
8.52	XRT	5×10^3	0.3 – 10 keV	$< 1.3\times 10^{-14}$ erg s^{-1}cm^{-2}	ATEL 2471
12.80	XRT	2.5×10^3	0.3-10 keV	$< 2.7\times 10^{-14}$ erg s^{-1}cm^{-2}	ATEL 2471
9.69	CARMA	19.8×10^3	95 GHz	$(-3.7\pm 1.8)\times 10^3$ μJy	ATEL 2473
10.14	Allen	4.8×10^3	3.09 GHz	$< 1.5\times 10^3$ μJy	ATEL 2472
17.69	EVLA	5.76×10^3	4.96 GHz	< 33 μJy	ATEL 2483
86.71	EVLA	3600	6 GHz	< 36μJy	This paper
276.9	EVLA	7200	4.96 GHz	< 35μJy	This paper
18.24	WSRT	28.8×10^3	4.8 GHz	< 126 μJy	ATEL 2479

NOTE. — Magnitudes are not corrected for Galactic extinction ($E(B-V)$ = 0.012 mag; Schlegel et al. 1998). P48 observations are calibrated to SDSS *r* (which is estimated to be on the AB system within ±0.01 mag), neglecting the color term. P48 errors

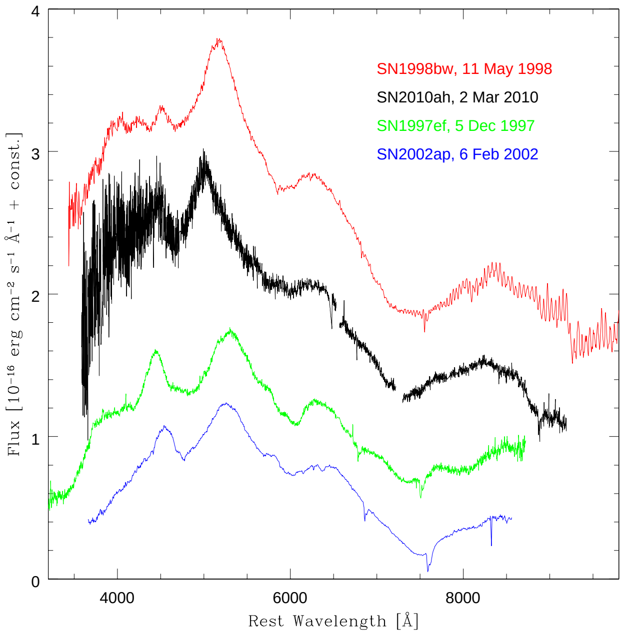

FIG. 3.— Gemini (black) spectrum of PTF 10bzf obtained on 2010 March 2, around the time of the *R*-band maximum. The spectrum is compared with that of SN 1997ef (green), SN 1998bw (red), SN 2002ap (blue) at similar epochs. Spectral data were retrieved from: Mazzali et al. (2000) for SN 19997ef; Patat et al. (2001) for SN 1998bw; Mazzali et al. (2002) for SN 2002ap. Main telluric lines have been removed from PTF 10bzf spectrum.

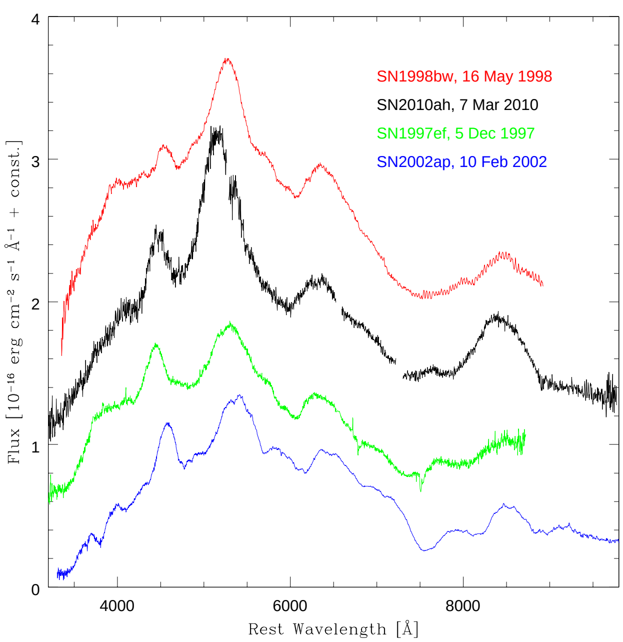

FIG. 4.— Keck (black) spectrum of PTF 10bzf obtained on 2010 March 7, about 5 days post *R*-band maximum. The spectrum is compared with that of SN 1997ef (green), SN 1998bw (red), SN 2002ap (blue) at similar epochs. Spectral data were retrieved from: Mazzali et al. (2000) for SN 19997ef; Patat et al. (2001) for SN 1998bw; Mazzali et al. (2002) for SN 2002ap. Main telluric lines have been removed from PTF 10bzf spectrum.

are reported in Table 2, where we have converted the 0.3–10 keV XRT count rates into fluxes assuming a photon spectrum of $N_\gamma \propto \nu^{-2}$, and correcting for Galactic absorption ($N_H \approx 10^{20}\,cm^{-2}$).

During the first epoch, PTF 10bzf was detected by *Swift*/UVOT (Kasliwal & Cenko 2010), and was observed to fade in the subsequent observation. The measured magnitudes in *Swift*/UVOT filters are reported in Table 2.

2.4. *Radio follow-up observations*

In the radio band, PTF 10bzf was followed-up by the Allen Telescope Array (Welch et al. 2009), by the Combined Array for Research in Millimeter-wave Astronomy (CARMA, Carpenter 2010), and by the Westerbork Synthesis Radio Telescope (WSRT, Kamble et al. 2010). No radio source was detected by any of these telescopes (Table 2).

The Expanded Very Large Array[26] (EVLA; Perley et al. 2009) provided the deepest upper-limit for a radio counterpart associated with PTF 10bzf (Chomiuk & Soderberg 2010, and Table 1). We analyzed the publicly available data of a second epoch observation of PTF 10bzf with EVLA (PI: A. Soderberg). This gives us a 3σ upper-limit comparable to the one obtained by Chomiuk & Soderberg (2010) during the first epoch (see Table 2). Finally, on 2010 November 27.49, we observed PTF 10bzf at 4.96 GHz, in a two-hour exposure, through an EVLA exploratory program (PI: A. Corsi)[27]. No radio source was detected at the SN position, the corresponding upper-limit is reported in Table 2.

3. COMPARISON WITH SN 1998BW AND GRB SEARCH

3.1. *Optical emission*

Figure 3 shows the spectrum of PTF 10bzf, compared with the spectra of several broad line Ic SNe. The spectrum of the PTF event is very similar to that of SN 1998bw around maximum light.

Our photometric monitoring program missed the photometric maximum. The peak apparent magnitude of PTF 10bzf was measured to be ≈ -18.34 mag, by performing synthetic photometry on the Gemini spectrum obtained at $\approx$ 7 days since discovery (see Table 2).

Observations, combined with theoretical models, have shown so far that only the brightest and most energetic Ic SNe produce a GRB (Mazzali et al. 2009). In Figure 2 and Table 1 we summarize the properties of the GRB-associated broad-line Ic SNe, of the broad-line Ic SNe 2003jd and 2002ap, and of the engine driven broad-line Ic SN 2009bb (Pignata et al. 2011; Soderberg et al. 2010). PTF 10bzf is brighter than the broad-line Ic SN 2002ap, comparable to the engine driven SN 2009bb at maximum light within the errors, but less bright than the broad-line Ic SN 2003jd and the GRB-associated SN 1998bw.

Although the peak epoch is not well known, we can estimate the ^{56}Ni mass in PTF 10bzf by interpolating between the *R*-band light-curves of SN 2002ap (for which $M_{^{56}\mathrm{Ni}} \approx 0.09\,M_\odot$, Mazzali et al. 2002) and SN 1998bw, (for which $M_{^{56}\mathrm{Ni}} \approx 0.5\,M_\odot$, Nakamura 1999; Nakamura et al. 2001). We find that for PTF 10bzf $M_{^{56}\mathrm{Ni}} \approx 0.20-0.25\,M_\odot$. The ^{56}Ni mass can also be estimated using the empirical relation derived by

[26] http://www.aoc.nrao.edu/evla/; The Very Large Array is operated by the National Radio Astronomy Observatory (NRAO), a facility of the National Science Foundation operated under cooperative agreement by Associated Universities, Inc.

[27] VLA/10C-227 - "Late time follow-up of Ic SN PTF 10bzf".

Drout et al. (2010) from the properties of a large sample of Ic SNe (including broad-line and engine driven SNe):

$$log(M_{^{56}\mathrm{Ni}}/M_{\odot}) \simeq -0.41 \times M_{\mathrm{R}} - 8.3 \quad (1)$$

where $M_{^{56}\mathrm{Ni}}$ is the mass of ^{56}Ni estimated using the formalism of Valenti et al. (2008) (see also Arnett 1982), and M_{R} is the extinction corrected peak magnitude in the R-band (see also Perets et al. 2010). For PTF 10bzf, using Equation (1), we get $M_{^{56}\mathrm{Ni}} \approx 0.2\,M_{\odot}$, compatible with what obtained by interpolation. This is comparable to SN 2002aj, associated with XRF 060218 (Mazzali et al. 2006b), and significantly less than all other GRB-associated SNe (see Table 1).

Estimating the kinetic energy requires modeling. However, we can use line velocity as a proxy for it. In Figure 3 and Figure 4 we show a spectroscopic sequence of broad-line Ic SNe, from 2002ap to 1998bw. The first (Figure 3) shows spectra near maximum light, the second (Figure 4) shows spectra obtained about 5 days after maximum. In addition, we show the only near-peak spectrum available of SN 1997ef, a broad-line SN without a GRB (Mazzali et al. 2000). We have ordered the SNe by peak luminosity. This ordering however reveals a sequence also in line velocity and blending. SN 1998bw has by far the broadest lines, SNe 1997ef and 2002ap have the narrowest lines, and PTF 10bzf is intermediate. Note for example that the peak near 4500Å which corresponds to a low opacity region where photons can more easily escape, is almost fully suppressed in SN 1998bw because of line broadening and blanketing. This is not the case for SN 1997ef, SN2002ap, and PTF 10bzf.

As shown by Mazzali et al. (2009) (see their Figure 4), the evolution of the Si II line velocity for SNe Ib/c, narrow- and broad-lined, with and without a GRB, is such that GRB-SNe have by far the highest velocity, and broad-line SNe have higher velocity than narrow-line SNe. PTF 10bzf seems to have a velocity intermediate between SN 2002ap and SN 1998bw.

Finally, ordering the SNe by velocity, gives an indication of a sequence in explosion kinetic energy. The ordering suggests that PTF 10bzf is intermediate in kinetic energy between non GRB-associated SNe like 2002ap or 1997ef on the one hand, and a GRB-associated SN like 1998bw on the other. Using the light-curve shape and the velocity to obtain the mass and kinetic energy of the explosion, as delineated by Arnett (1982), we obtain for PTF 10bzf: $M = 6 \pm 2\ \mathrm{M}_{\odot}$, $E_{\mathrm{K}} = (15 \pm 5) \times 10^{51}$ erg. These values are not very different from SN1997ef, for which a progenitor mass of 35 $\mathrm{M}_{\odot}$ was estimated (Mazzali et al. 2000). We thus conclude that PTF 10bzf probably lacks the mass and energy required to initiate a GRB.

3.2. *X-ray upper limit*

The X-ray flux of GRB 980425 about 1 day after the burst was $\approx 3 \times 10^{-13}\,\mathrm{erg\,s^{-1}cm^{-2}}$, and it declined at a rate of $\propto t^{-0.2}$ (Nakamura 1999; Pian et al. 2000). The *Swift*/XRT upper limit for PTF 10bzf at 8.5 days, constrains any X-ray source associated with PTF 10bzf to have a flux $< 1.3 \times 10^{-14}$ erg s^{-1}cm^{-2}, i.e. at least a factor of ≈ 15 lower than the X-ray flux of SN 1998bw, rescaled at a similar epoch using a $t^{-0.2}$ decay.

3.3. *Early time ($t \lesssim 20$ days) radio upper-limits*

The novelty of SN 1998bw was in the discovery of prompt radio emission just a few days after GRB 980425

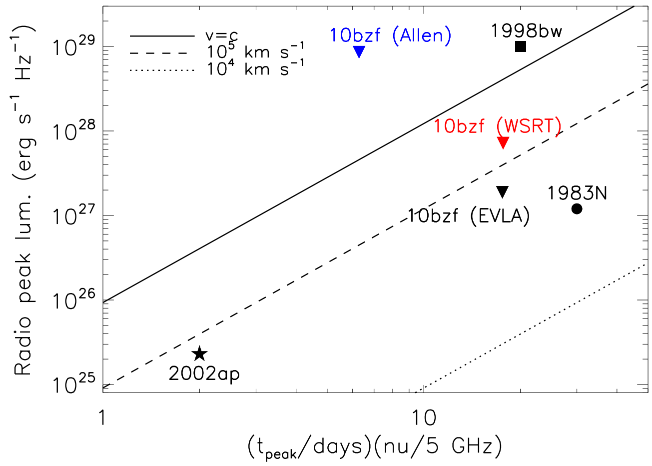

FIG. 5.— Constraints on approximate expansion velocity derived from the early-time Allen telescope (blue triangle), WSRT (red triangle), and EVLA (black triangle) radio upper-limits on PTF 10bzf (see Table 2 and Equation 4), compared with similar constraints obtained from the radio detections of SN 1998bw (black square), SN 1983N (black dot), and SN 2002ap (black star) (see Figure 2 in Berger et al. 2003, for comparison). As evident, SN 1998bw with $v_r \sim c$ remains an exception. The Allen upper-limit on PTF 10bzf around its peak time (~ 10 days since discovery, see Table 2) does not exclude a relativistic expansion. However, v~ c is indeed excluded by the radio upper-limits obtained about a week later by EVLA and WSRT.

(Kulkarni et al. 1998). The rapid rise of the radio light-curve indicated that the SN explosion time coincided with the GRB to $\sim$ 1 day. The brightness temperature suggested that the radio photosphere moved relativistically ($\Gamma \geq 2$), with a total energy of $\sim 10^{50}$ erg (Li & Chevalier 1999), about two orders of magnitude less than the total kinetic energy of the explosion, which was estimated to be of $\sim 3 \times 10^{52}$ erg (Iwamoto et al. 1998). None of these last features, together with the spatial and temporal association with a GRB, were ever observed for a nearby SN before SN 1998bw, thus suggesting the presence of a central engine powering this explosion.

At a redshift of $z = 0.0498$, the deepest early time radio upper-limit for PTF 10bzf was obtained by Chomiuk & Soderberg (2010). This sets a limit of on the spectral luminosity of $L_{5\,\mathrm{GHz}} < 1.6 \times 10^{27}\,\mathrm{erg\,s^{-1}\,Hz^{-1}}$, at about three weeks after the explosion. This is $\approx$ 20 times lower than the radio luminosity observed on a similar timescale for the Ic SN 1998bw and SN 2009bb (Soderberg et al. 2010), the only two SNe which showed clear evidence for energetic and mildly-relativistic outflows (Chomiuk & Soderberg 2010).

Using the early-time radio upper-limit, we constrain the mean expansion speed v_r of the radio photosphere. Under the reasonable assumption that radio emission arises from a synchrotron spectrum with $\nu_{\mathrm{a}} \sim \nu_{\mathrm{p}}$ (where ν_{a} is the self-absorption frequency and ν_{p} the peak frequency), the peak-time t_{p}, and peak-luminosity L_{p} of the radio emission directly measure the average expansion speed (Berger et al. 2003; Chevalier 1998). In fact, since the peak happens at the transition from optically thick to optically thin behavior, at such time $L_{\mathrm{thin}} \sim L_{\mathrm{thick}} \sim L_{\mathrm{p}}$, where (Chevalier 1998):

$$L_{\mathrm{thick}} \propto R_{\mathrm{r}}^2 B^{-1/2} \nu_{\mathrm{p}}^{5/2}\,; \qquad L_{\mathrm{thin}} \propto R_{\mathrm{r}}^3 B^{7/4} \nu_{\mathrm{p}}^{-3/4}\,. \quad (2)$$

Here B is the magnetic field, and R_{r} is the size of the radio photosphere. By imposing:

$$L_{\rm thin} = L_{\rm thick}\,; \qquad L_{\rm thin} = L_{\rm p}\,, \tag{3}$$

we have two conditions that allow us to determine the two unknown parameters B and $R_{\rm r}$. Thus, measuring $\nu_{\rm p}$, $t_{\rm p}$ and $L_{\rm p}$, we can constrain the size of the radio source $R_{\rm r}$, and estimate the mean expansion velocity as $v_r \sim R_r/t_p$ (Berger et al. 2003; Chevalier 1998):

$$v_{\rm r} \sim 3.1{\times}10^4 \left(\frac{L_{\rm p}}{10^{26}{\rm erg\,s^{-1}}}\right)^{17/36} \left(\frac{t_{\rm p}}{10\,{\rm days}}\right)^{-1} \left(\frac{\nu_p}{5\,{\rm GHz}}\right)^{-1} {\rm km\,s^{-1}}\,. \tag{4}$$

Figure 5 shows $L_{5\,{\rm GHz}}$ at peak versus $t_{\rm p}\nu_{\rm p}$ for different values of $v_{\rm r}$, compared with the Allen telescope, WSRT and EVLA upper-limits on PTF 10bzf. Assuming that the radio emission peaked at $\approx$ 18 days, the WSRT and EVLA observations constrain the expansion velocity to be less than 10^5 km s^{-1}.

Estimating the expansion velocities for non-detections has the caveat that the radio peak epoch is in reality unknown. However, as noted by Berger et al. (2003), observations performed at $\sim$ 10 − 20 days since explosion, sample the radio peak time of Ic SN reasonably well. E.g. SN 1983N peaked in radio at $\sim$ 30 days after explosion, while the radio light-curve of SN 1998bw showed a double-peak profile, with the first peak around 10 days since explosion, and the second around 30 days after explosion. This justifies our use of radio upper-limits taken within $\approx$ 3 weeks since discovery to constrain the expansion speed.

3.4. *Late time ($t \gtrsim 20$ days) radio upper-limits*

In the context of the fireball model, the emission from an off-axis GRB is expected to be visible in the radio band long past the GRB explosion (at timescales of the order of $\sim$ 1 yr, see Levinson et al. 2002). In fact, at sufficiently late times, the relativistic fireball is expected to enter the sub-relativistic phase, during which the jet starts spreading, rapidly intersecting the viewer's line of sight as the ejecta approaches spherical symmetry.

To model the late-time radio emission from an off-axis GRB during the non-relativistic phase, we use the analytical model by Waxman (2004) for a fireball expanding in a wind medium (see e.g. Levinson et al. 2002, for the constant ISM case). In this model the radio luminosity is approximated as (see also Soderberg et al. 2006b):

$$L_{\rm r} \sim 2.1\times10^{29} \left(\frac{\epsilon_{\rm e}\epsilon_{\rm B}}{0.01}\right)^{3/4} \left(\frac{\nu}{10\,{\rm GHz}}\right)^{-\frac{(p-1)}{2}} \left(\frac{t}{t_{\rm NR}}\right)^{-3/2} \times A_*^{9/4} E_{51}^{-1/2}\ {\rm erg\,s^{-1}\,Hz^{-1}}, \tag{5}$$

where E_{51} is the beaming-corrected ejecta energy, A_* defines the circumstellar density in terms of the progenitor mass loss-rate $\dot{M}$ and wind velocity $v_{\rm w}$ such that $\dot{M}/4\pi v_{\rm w} = 5\times10^{11} A_*$ g cm^{-1} (Waxman 2004; Soderberg et al. 2006b), and:

$$t_{\rm NR} \sim 0.3 \left(\frac{E_{51}}{A_*}\right)\ {\rm yr}, \tag{6}$$

is the time of the non-relativistic transition. By imposing $t_{\rm NR} \lesssim t_{\rm obs}$ and $L_r \lesssim L_{\rm obs}$, we can use the EVLA observations of PTF 10bzf (see Table 2) to obtain the exclusion regions shown in Figure 6. From such a Figure we conclude

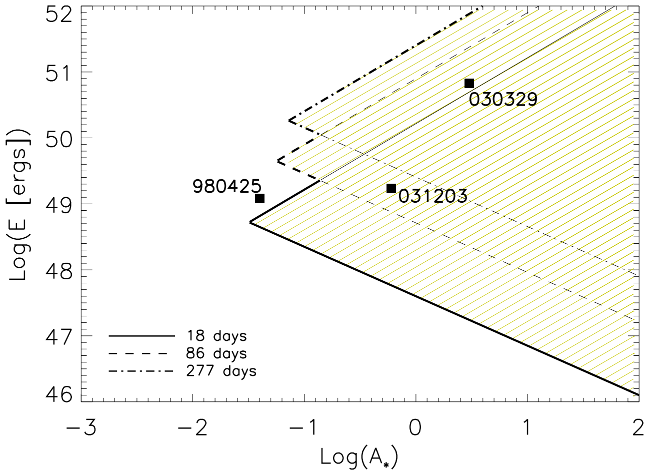

FIG. 6.— Off-axis emission from a GRB explosion associated with PTF 10bzf. The yellow shadowed regions mark the portion of the energy-density plane excluded by the first, second, and third epoch EVLA observations, respectively (see Table 2). As evident from the figure, late-time radio observations are fundamental to exclude the higher energy - higher density region of the energy-density plane. This region contains the most common values of energies and densities ($E_{51} \sim 1-10$ and $A_* \sim 1$) observed for long GRBs. We also show for comparison some of the parameters estimated from broad-band modeling of GRBs associated with SNe (980425, 030329, and 031203, see Soderberg et al. 2006b, and references therein).

that an off-axis GRB explosion with energy and density comparable to the ones of the SN-associated GRB 030329 and GRB 031203, is excluded for PTF 10bzf.

3.5. *Search for γ-rays*

We searched for a possible GRB in coincidence with PTF 10bzf using the IPN data. We searched for bursts with a localization error-box including PTF 10bzf. Since the exact explosion epoch of PTF 10bzf is not known, we searched in a time-window extending from 2010 February 12 to 2010 February 23 (the discovery day of PTF 10bzf). We conservatively extend such a time window to include one full week prior to our last non-detection of PTF 10bzf. Therefore, our time window starts $\approx$ 11 days before the SN discovery (i.e. $\approx$ 18 days before its R-band maximum light).

For comparison, we note that the engine driven SN 2009bb reached its maximum light about two weeks after the estimated explosion date (Soderberg et al. 2010), evolving somewhat faster than SN 1998bw in the pre-peak phase (Pignata et al. 2011). As evident from Figure 2, our last upper-limit on 2010 February 19 ($R > 21.4$) indicates that also PTF 10bzf probably evolved more rapidly than SN 1998bw in its pre-peak phase. Using the R-band light curve as a proxy for $L(t)$, and assuming a pre-peak luminosity evolution $L(t) \propto (t-t_0)^{1.8}$ (where t_0 is the explosion time, see e.g. Pignata et al. 2011), t_0 should be set to $\approx$ 2010 February 18.8 to account for the $\gtrsim$ 2.4 mag drop observed between our last non-detection of PTF 10bzf, and its discovery. We then conservatively extend our time interval for the GRB search to one week prior to 2010 February 19.

Between 2010 February 12 and 2010 February 23, a total of fourteen confirmed bursts were detected by the spacecrafts of the interplanetary network (IPN[28]: Mars Odyssey, Konus-Wind, RHESSI, INTEGRAL (SPI-ACS), *Swift*-BAT, MESSENGER, Suzaku, AGILE, and Fermi (GBM)). Here con-

[28] http://www.ssl.berkeley.edu/ipn3/

firmed means that they were observed by more than one detector on one or more spacecraft, and could be localized at least coarsely.

The localization accuracies of these fourteen bursts varied widely, but none of them was found to be consistent with the position of PTF 10bzf. One burst was observed by the Fermi GBM alone (error circles with 1σ statistical-only error radii of 10.5 degrees), while other five were observed by the GBM and other spacecrafts. Four events were observed by a distant IPN spacecraft, and could be triangulated to annuli or error boxes with dimensions as small as $\sim 10'$. Five GRBs were observed within the coded field of view of the *Swift* BAT ($3'$ initial localization accuracy), and in some cases by other IPN spacecrafts as well.

PTF 10bzf is not spatially associated with any of these GRBs. The total area of the localizations of the fourteen confirmed bursts, containing the 3σ error regions, was ≈ 1.3 *sr*. Therefore, there is only $\approx 10\%$ chance coincidence between these bursts and PTF 10bzf.

Next, based on our GRB sample, we can put a limit on the fluence of any GRB associated with PTF 10bzf. We considered three distinct sets of events: IPN bursts, Fermi GBM-only bursts, and *Swift* BAT-only bursts. The IPN is sensitive to bursts with fluences down to about 6×10^{-7} erg cm^{-2} (50% efficiency - see Hurley et al. 2010), and observes the entire sky with a temporal duty cycle close to 100%. The Fermi GBM detects bursts down to a $8-1000$ keV fluence of about 4×10^{-8} erg cm^{-2}, and observes the entire unocculted sky (≈ 8.8 sr) with a temporal duty cycle of more than 80%. The weakest burst observed by the BAT had a 15-150 keV fluence of 6×10^{-9} erg cm^{-2}, and the BAT observes a field of view of about 2 sr with a temporal duty cycle of about 90%.

If the SN produced a burst below the IPN threshold, and above the Fermi one, it is possible that both *Swift* and Fermi did not detect it: considering their spatial and temporal coverages, the non-detection probabilities are about 0.86 and 0.44, respectively. Finally, if the SN produced a burst below the Fermi threshold, but above the *Swift* one, the non-detection probability is about 0.86. We note that a burst with an isotropic energy release comparable to that of the sub-energetic GRB 980425, $E_{\rm iso} \approx 6\times10^{47}$ ergs, placed at the distance of PTF 10bzf, would be observed with a fluence of $\approx 10^{-7}$ erg cm^{-2}, which is below the IPN threshold, but above the Fermi GBM one.

4. CONCLUSION

We presented the discovery of PTF 10bzf, a broad-line type Ic SN detected by PTF. We obtained multi-wavelength follow-up observations of this SN, we compared its properties with those of other SNe associated with GRBs, and put limits on any associated GRB using the IPN sample.

While PTF 10bzf shows some spectral similarities with SN 1998bw, its *R*-band and radio luminosities are much lower, with no clear evidence for a relativistic expansion speed. The spectral properties of PTF 10bzf suggest that this SN is intermediate, in terms of explosion kinetic energy, between non-GRB associated SNe like 2002ap or 1997ef, and GRB-associated SNe like 1998bw. A search for γ-rays using the IPN sample, gives no GRB with a position consistent with this SN, in a time-window extending to a full week prior to our last non-detection of the source. We thus conclude that PTF 10bzf probably lacks the mass and energy required to initiate a GRB.

Despite the fact that PTF 10bzf does not show evidence for being associated with a nearby GRB, the discovery and follow-up of broad-line Ic SNe remains a fundamental tool to investigate the GRB-SN connection. Broad-line Ic SNe are rare, and they are the only type of SNe which have confirmed associations with GRBs. Therefore, it is crucial to study them, and determine how the GRB-associated SNe differ from the other broad-line Ic SN. PTF is a project able to discover and classify about ten broad-line Ic SNe per year, thus allowing to construct a large sample of SNe which are unique broad-line Ic.

The search for SNe associated with nearby (non γ-ray triggered) GRBs, is particularly relevant also in the light of multi-messenger astronomy. In an era in which ground-based gravitational wave detectors like LIGO[29] and Virgo[30] are approaching their advanced configurations, nearby GRBs represent promising candidates for the detection of gravity waves (e.g. Kobayashi & Mészáros 2003; Kokkotas 2004; Woosley & Bloom 2006; Piro & Pfahl 2007; Corsi & Mészáros 2009; Ott 2009, and references therein). The simultaneous operation of facilities like PTF and LIGO may open, in the forthcoming years, a unique opportunity for this kind of multi-messenger searches (e.g. Bloom et al. 2009; Smith et al. 2009; Stamatikos et al. 2009; Shawhan 2010, and references therein).

The National Energy Research Scientific Computing Center, which is supported by the Office of Science of the U.S. Department of Energy under Contract No. DE-AC02-05CH11231, provided staff, computational resources and data storage for this project.
E. O. O. is supported by an Einstein Fellowship and NASA grants. D. P. is supported by an Einstein fellowship.
The Weizmann Institute PTF partnership is supported in part by grants from the Israeli Science Foundation (ISF) to A.G. Joint work by the Weizmann and Caltech groups is supported by a grant from the Binational Science Foundation (BSF) to A.G. and S.R.K. A.G. acknowledges further support from an EU/FP7 Marie Curie IRG fellowship and a research grant from the Peter and Patricia Gruber Awards.
The National Radio Astronomy Observatory is a facility of the National Science Foundation operated under cooperative agreement by Associated Universities, Inc.
LAIWO, a wide-angle camera operating on the 1-m telescope at the Wise Observatory, Israel, was built at the Max Planck Institute for Astronomy (MPIA) in Heidelberg, Germany, with financial support from the MPIA, and grants from the German Israeli Science Foundation for Research and Development, and from the Israel Science Foundation.
LIGO was constructed by the California Institute of Technology and Massachusetts Institute of Technology with funding from the National Science Foundation.
We are grateful to IPN collaborators S. Golenetskii, R. Aptekar, E. Mazets, D. Frederiks, and T. Cline for the Konus data; to M. Briggs and C. Meegan for the Fermi data; to T. Takahashi, Y. Terada, M. Tashiro, Y. Fukazawa, T. Murakami, M. Ohno, and K. Makishima for the Suzaku data; to S. Barthelmy, N. Gehrels, H. Krimm, and D. Palmer for the Swift data; to D. Golovin, A. Kozyrev, M. Litvak, A. Sanin, C. Fellows, K. Harshman, and R. Starr for the Odyssey

[29] www.ligo.org
[30] www.virgo.infn.it

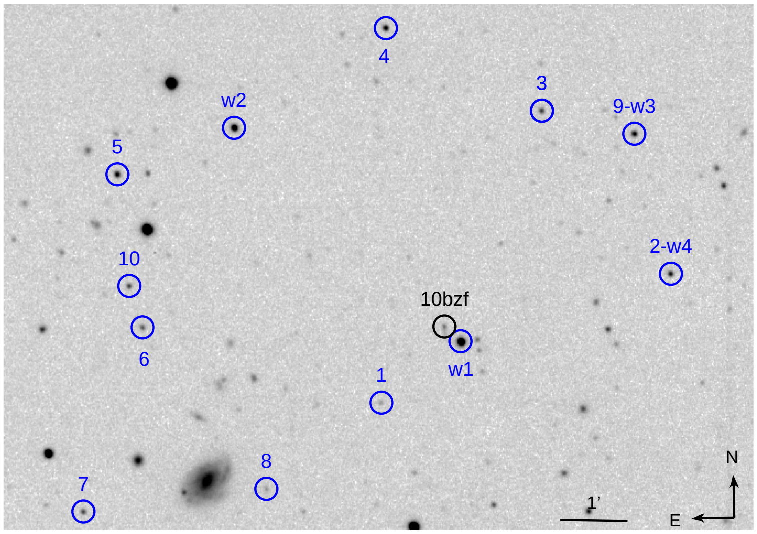

FIG. 7.— Image of the field of PTF 10bzf at discovery. For clarity purposes, a circle of 10″ radius marks the position of PTF 10bzf and of ten reference stars (1-10) selected to calibrate P48 R magnitudes to SDSS r. We also mark (w1-w4) – the four references stars used for calibration of the Wise photometry. The SN is located at RA=11:44:02.99 and Dec=+55:41:27.6 (J2000), and its host galaxy, located at RA=11:44:02.98 and Dec=+55:41:22.5, is also visible.

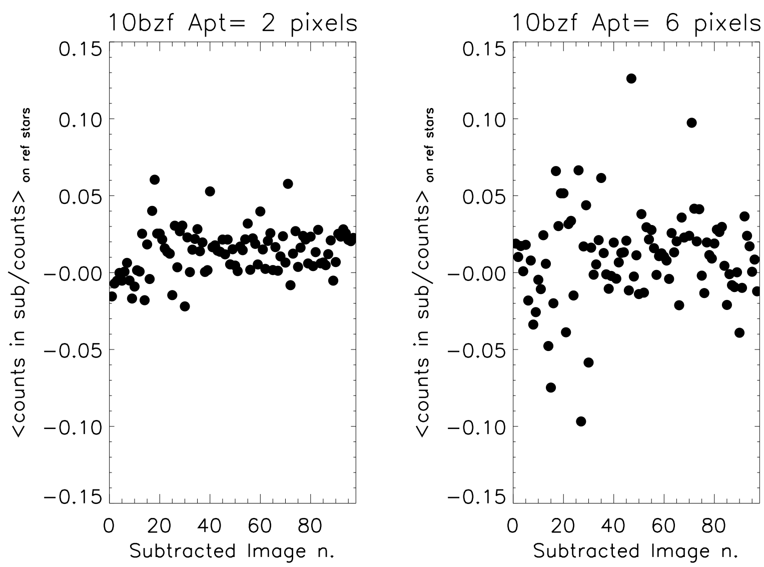

FIG. 8.— Δ_j(2 pixels) and Δ_j(6 pixels) for the 97 images. It is evident that an aperture radius of 2 pixels introduces, overall on the 97 images, a smaller subtraction error than a 6 pixels aperture.

data; and to A. von Kienlin and X. Zhang for the INTEGRAL data. KH acknowledges support from the following NASA sources: NNX09AV61G (Suzaku), NNX10AI23G (Swift), NNX10AU34G (Fermi), and NNX07AR71G (MESSENGER).

APPENDIX

P48 PHOTOMETRY

Image subtraction, aperture correction and calibration to SDSS r

We performed image subtraction on the P48 images (e.g. Alard & Lupton 1998). After the image subtraction step, we registered all images to the same reference frame (which, for convenience, was chosen to be the one of the first of the 97 images). This was done by using the "wregister" tool available in IRAF[31]. Next, we selected 10 reference stars in the field of PTF 10bzf (see Figure 6), and performed aperture photometry of these stars for both sets of 97 images and 97 subtracted images. Aperture photometry was done with the "phot" tool available in IRAF V2.14, varying the aperture radius r_{apert} in the range 1-10 pixels. For each of the pairs of image / subtracted image, we calculated the mean, over the 10 reference stars, of the ratios between the

[31] IRAF is distributed by the National Optical Astronomy Observatory, which is operated by the Association for Research in Astronomy, Inc., under cooperative agreement with the National Science Foundation.

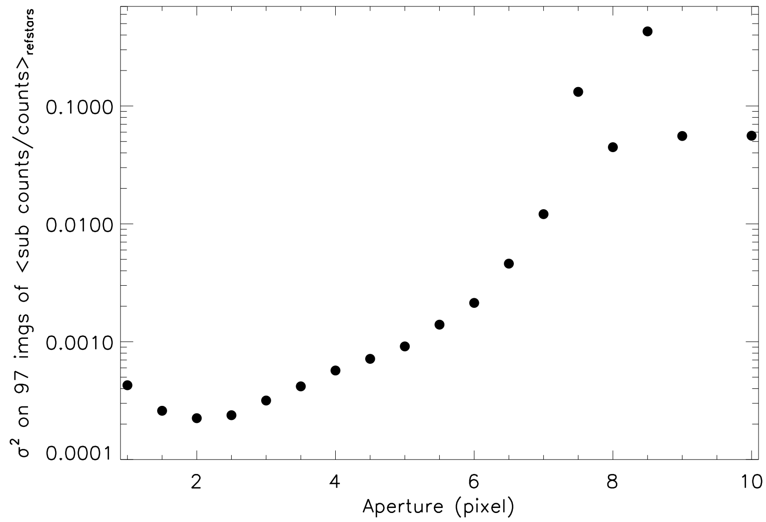

FIG. 9.— $\sigma^2_{\Delta}(r_{apert})$ as a function of aperture.

counts of a reference star in the subtracted image, $C^i_{sub,j}$, and the counts of the same reference star in the (non-subtracted) image, $C^i_{\mathrm{image},j}$. This was computed for each aperture radius (r_{apert}):

$$\Delta_j(r_{\mathrm{apert}}) = \frac{1}{N}\sum_{i=1}^{N}\frac{C^i_{sub,j}(r_{\mathrm{apert}})}{C^i_{\mathrm{image},j}(r_{\mathrm{apert}})}\ , \tag{A1}$$

where i is the reference star index, $N = 10$ is the total number of reference stars, and $j = 1 - 97$ is the image index. $\Delta_j(r_{apert})$ is thus a function of the selected aperture radius, and would be equal to zero in an ideal and noiseless subtraction process. In reality, because of systematic and statistical noise, this does not happen. Thus, $\Delta_j(r_{apert})$, can be considered as an estimate of the goodness of the subtraction, and later on regarded as a bias in the SN flux in the subtracted images, introduced by the subtraction process. For comparison, in Figure 8 we show Δ_j(2 pixels) and Δ_j(6 pixels) for the 97 images. It is evident that an aperture radius of 2 pixels introduces, overall on the 97 images, a smaller subtraction error than for a 6 pixels. Therefore, we fixed the aperture to a value $r_0 = 2$ pixels that minimizes the r.m.s. of Δ_j on the 97 images (see Figure 9). We then computed the SN counts, $C^{SN}_j(r_0)$, as:

$$C^{SN,corr}_j(r_0) = C^{SN}_j(r_0) - \Delta_j(r_0)C^{SN}_j(r_0) \tag{A2}$$

The error associated with this correction has been estimated as:

$$\sigma^2_{\Delta_j}(r_0) = \frac{1}{N}\sum_{i=1}^{N}\left[\frac{C^i_{sub,j}(r_0)}{C^i_{\mathrm{image},j}(r_0)} - \Delta_j(r_0)\right]^2 \tag{A3}$$

and added in quadrature to the calibration and background errors.

REFERENCES

Alard, C., & Lupton, R. H. 1998, ApJ, 503, 325
Arcavi, I., et al. 2010, ApJ, 721
Arnett, W. D. 1982, ApJ, 253, 785
Berger, E., et al. 2003, ApJ, 599, 408
Bloom, J. S., et al. 2009, ArXiv e-prints 0902.1527
Carpenter, J. M. 2010, The Astronomer's Telegram, 2473, 1
Chevalier, R. A. 1998, ApJ, 499, 810
Chomiuk, L., & Soderberg, A. 2010, The Astronomer's Telegram, 2483, 1
Corsi, A., & Mészáros, P. 2009, ApJ, 702, 1171
Della Valle, M., et al. 2006, Nature, 444, 1050
Deng, J., et al. 2005, ApJ, 624, 898
Drout, M. R., et al. 2010, ArXiv 1011.4959
Filippenko, A. V. 1997, ARA&A, 35, 309
Foley, R. J., et al. 2003, PASP, 115, 1220
Fynbo, J. P. U., et al. 2006, Nature, 444, 1047
Gal-Yam, A., et al. 2004, ApJL, 609, L59
Gal-Yam, A., et al. 2006a, Nature, 444, 1053
Gal-Yam, A., et al. 2006b, ApJ, 639, 331
Gal-Yam, A., Maoz, D., Guhathakurta, P., & Filippenko, A. V. 2008, ApJ, 680, 550
Gal-Yam, A., Ofek, E. O., & Shemmer, O. 2002, MNRAS, 332, L73
Galama, T. J., et al. 1998, Nature, 395, 670
Guetta, D., & Della Valle, M. 2007, ApJL, 657, L73
Hjorth, J., et al. 2003, Nature, 423, 847
Hook, I. M., et al. 2004, PASP, 116, 425
Hurley, K., et al. 2010, in Italian Phys. Soc. Conf. Proc., ed. Eds. G. Chincarini, P. D'Avanzo, R. Margutti, and R. Salvaterra, Vol. 102, 529
Iwamoto, K., et al. 1998, Nature, 395, 672
Jordi, K., Grebel, E. K., & Ammon, K. 2006, A&A, 460, 339
Kamble, A. P., et al. 2010, The Astronomer's Telegram, 2479, 1
Kasliwal, M. M., & Cenko, S. B. 2010, The Astronomer's Telegram, 2471, 1
Kobayashi, S., & Mészáros, P. 2003, ApJ, 589, 861
Kokkotas, K. D. 2004, Classical and Quantum Gravity, 21, 501
Kulkarni, S. R., et al. 1998, Nature, 395, 663
Law, N. M., et al. 2009, PASP, 121, 1395
Levinson, A., et al. 2002, ApJ, 576, 923
Li, Z., & Chevalier, R. A. 1999, ApJ, 526, 716
Liang, E., Zhang, B., Virgili, F., & Dai, Z. G. 2007, ApJ, 662, 1111
MacFadyen, A. I., & Woosley, S. E. 1999, ApJ, 524, 262
Malesani, D., et al. 2004, ApJL, 609, L5

Matheson, T., et al. 2003, ApJ, 599, 394
Mazzali, P. A., et al. 2002, ApJL, 572, L61
Mazzali, P. A., et al. 2005, Science, 308, 1284
Mazzali, P. A., et al. 2006a, Nature, 442, 1018
Mazzali, P. A., et al. 2006b, ApJ, 645, 1323
Mazzali, P. A., Deng, J., Hamuy, M., & Nomoto, K. 2009, ApJ, 703, 1624
Mazzali, P. A., Iwamoto, K., & Nomoto, K. 2000, ApJ, 545, 407
Mészáros, P. 2006, Reports on Progress in Physics, 69, 2259
Nakamura, T. 1999, ApJL, 522, L101
Nakamura, T., Mazzali, P. A., Nomoto, K., & Iwamoto, K. 2001, ApJ, 550, 991
Norris, J. P. 2002, ApJ, 579, 386
Ofek, E. O., et al. 2007, ApJ, 662, 1129
Ofek, E. O., et al. 2010, The Astronomer's Telegram, 2470, 1
Ott, C. D. 2009, Classical and Quantum Gravity, 26, 204015
Patat, F., et al. 2001, ApJ, 555, 900
Perets, H. B., et al. 2010, Nature, 465, 322
Perley, R., et al. 2009, IEEE Proceedings, 97, 1448
Pian, E., et al. 2000, ApJ, 536, 778
Pian, E., et al. 2006, Nature, 442, 1011
Pignata, G., et al. 2011, ApJ, 728, 14
Piro, A. L., & Pfahl, E. 2007, ApJ, 658, 1173
Podsiadlowski, P., et al. 2004, ApJ, 607, L17
Rau, A., et al. 2009, PASP, 121, 1334
Schlegel, D. J., Finkbeiner, D. P., & Davis, M. 1998, ApJ, 500, 525
Shawhan, P. 2010, APS Meeting Abstracts, 4002
Smith, J., et al. 2009, in Bulletin of the AAS, Vol. 41, Bulletin of the American Astronomical Society, 443
Soderberg, A. M., et al. 2006a, Nature, 442, 1014
Soderberg, A. M., et al. 2010, Nature, 463, 513
Soderberg, A. M., Nakar, E., Berger, E., & Kulkarni, S. R. 2006b, ApJ, 638, 930
Stamatikos, M., et al. 2009, in astro2010: decadal Survey, ArXiv 0902.3022, 284
Starling, R. L. C., et al. 2010, ArXiv e-prints 1004.2919
Valenti, S., et al. 2008, MNRAS, 383, 1485
Virgili, F. J., Liang, E., & Zhang, B. 2009, MNRAS, 392, 91
Waxman, E. 2004, Apj, 602, 886
Welch, J., et al. 2009, IEEE Proceedings, 97, 1438
Woosley, S. E., & Bloom, J. S. 2006, ARA&A, 44, 507
York, D. G., et al. 2000, ApJ, 120, 1579